Physics Letters A 377 (2013) 1725–1735

Contents lists available at SciVerse ScienceDirect

Physics Letters A

www.elsevier.com/locate/pla

Characteristics of dithering cycles during the L–I–H transition on Experimental Advanced Superconducting Tokamak (EAST)

T. Zhang, X. Gao *, S.B. Zhang, Y.M. Wang, X. Han, Z.X. Liu, B.L. Ling

EAST Team

Institute of Plasma Physics, Chinese Academy of Sciences, PO Box 1126, Hefei, Anhui 230031, People's Republic of China

ARTICLE INFO

Article history:
Received 13 January 2013
Received in revised form 19 March 2013
Accepted 1 May 2013
Available online 6 May 2013
Communicated by F. Porcelli

Keywords:
L–I–H transition
I phase
Dithering cycle
Edge turbulence

ABSTRACT

An intermediate phase (labeled I phase) with dithering cycles between the L-mode and H-mode has been observed and experimentally characterized on Experimental Advanced Superconducting Tokamak (EAST). A typical characteristics of the I phase is that the D_α signal, edge density fluctuation level and edge radiation show several kHz periodical oscillation. The analysis shows that the dithering event is at least 2 cm inside the separatrix and extends into the scrape-off layer (SOL) region. It is found that this dithering occurs in plasma with double null (DN) or upper single null (USN) configuration and cannot be observed in plasma with lower single null (LSN) configuration where the ion $B \times \nabla B$ drift direction is 'unfavorable', i.e. away from the X-point, in this device. The dithering cycle length (Δt_{dither}) has no clear dependence on the heating power. Both stored energy and density increase during the dithering phase and the increasing rates decrease with Δt_{dither}. The evolution of density profiles during the L–I–H transition is analyzed and presented.

1. Introduction

Since the discovery of high confinement mode (H-mode) in ASDEX tokamak [1], lots of work has been done to understand the H-mode physics and significant progresses have been made in experiment [2] and theory [3]. The L–H transition power threshold for next step fusion device, e.g. ITER, is still uncertain since the physics involved in this transition process has not yet been fully understood [2]. It is believed that the confinement improvement in H-mode is due to suppression or reduction of turbulent transport. There are clear experimental evidences for a fast reduction in the level of edge turbulence during the L–H transition [4–8]. The earliest theories attributed the turbulence suppression and the transition to the increase of the radial electric field (E_r) [9–11] and its associated $E_r \times B$ drift (mean flow) [12]. More recently, the predator–prey model [13,14] reveals a complex interaction between zonal flows (ZFs), turbulence and the mean flow. As discussed in Ref. [15], the L–H transition threshold power is lowered by including the evolution of ZFs self-consistently. When the ZFs are incorporated in a L–H transition model [14], the predator–prey type competition between turbulence and ZFs will result in a limit cycle oscillation (LCO) phase where turbulent fluctuation level is modulated by a low frequency E_r oscillation.

In experiments, dithering cycles with several kHz quasi-periodic evolution of D_α and edge T_e were first observed on ASDEX-Upgrade (AUG) [16,17]. During the cycles, only a narrow region of ~2 cm inside the separatrix was affected and the transport coefficients in this region were periodically switched between L- and H-values. An intermediate regime (IM-mode) was found on DIII-D between the L- and H-modes [18,19]. The IM-mode is characterized by edge periodic instability bursts which clamped the density but allowed improvement of the thermal confinement resulting in the gradual increase of temperature and no change of density. Recent observation in AUG showed that an intermediate phase (I phase) usually occurred when the heating power is close to the L–H transition power threshold. In the I phase, the $E_r \times B$ flow and turbulence level were periodically modulated at a frequency of 2–4 kHz and a limit-cycle behavior between geodesic acoustic mode (GAM) with a frequency ~19 kHz and the background turbulence was observed during the enhanced turbulence state [20]. An oscillation with a limit-cycle behavior between ZF with frequency ~2 kHz and background turbulence preceding L–H transition was also observed in DIII-D [21]. Similar oscillations also appear on H-1 heliac [22] and TJ-II stellarator [23]. On EAST tokamak, a quasi-periodic E_r oscillation with a frequency about 4 kHz and a modulation in edge turbulence preceding the L–H transition have been observed at marginal input power [24]. The oscillation amplitude, typically only of ~3% in target D_α signal, is much smaller than those mentioned above. In the new campaign of EAST in 2012 spring, the previous water cooled graphite first wall was

* Corresponding author. Tel.: +86 551 65593108; fax: +86 551 65591310.
E-mail address: xgao@ipp.ac.cn (X. Gao).

0375-9601/$ – see front matter
http://dx.doi.org/10.1016/j.physleta.2013.05.001

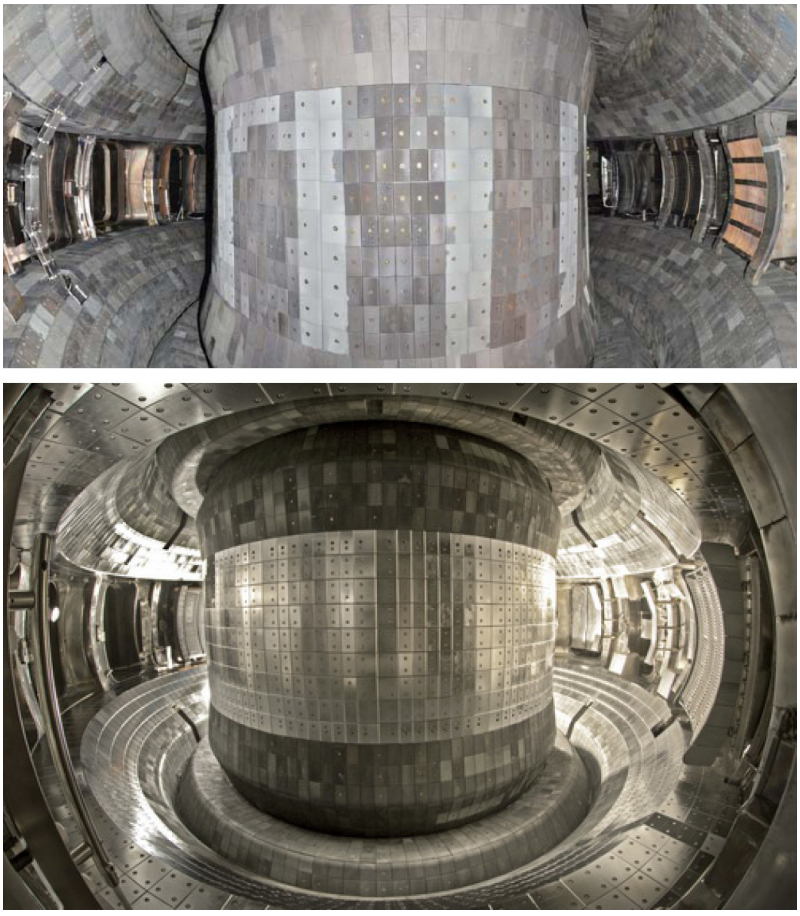

Fig. 1. Views of in-vessel with water-cooled graphite wall (upper picture) and with molybdenum wall (lower picture) on EAST.

changed to molybdenum wall and an intermediate phase (labeled I phase) displaying dithering cycles with a much larger oscillating amplitude (∼30% in D_α signal) between L- and H-modes has been observed. In this Letter, we will experimentally characterize this dithering cycles on EAST tokamak.

This Letter is organized as follows: in Section 2, the observation and localization of the dithering cycle on EAST tokamak is presented. The occurrence of the dithering cycle in the operational window of EAST is described in Section 3. The plasma evolution, mainly the density evolution, during the dithering phase is characterized in Section 4. Lastly, a discussion and summary on the results are given in Section 5.

2. Observation and localization of the dithering cycles during L–I–H transition

EAST, a non-circular full superconducting tokamak with a major radius (R) of 1.75 m and a minor radius (a) of 0.45 m, was designed for steady state divertor operation for a duration of 1000 s. The device can be operated in multi-configurations including single null (SN) divertor, double-null (DN) divertor or circular configuration with a limiter. The H-mode was achieved on EAST tokamak in 2010 [25] and the confinement during ELMy H-mode has been studied [26]. In 2012 spring campaign, the material for first wall has been changed from graphite to molybdenum (see Fig. 1). All the discharges presented in this Letter are from this campaign and operated with working gas of deuterium, plasma current (I_p) from −300 kA to −500 kA and toroidal magnetic field (B_t at $R = 1.85$ m) of −1.9 T. Here, the minus sign of I_p and B_t indicate that both quantities are anticlockwise viewed from the top of the device. Therefore, the ion $B \times \nabla B$ drift direction is towards the X-point in the upper single null (USN) configuration, i.e. so-called 'favorable' direction, while this drift direction is away from the X-point in the lower single null (LSN) configuration, i.e. 'unfavorable' direction. The H-mode is achieved by applying the lower hybrid wave (LHW) and ion cyclotron resonance heating (ICRH) after wall conditioning by lithium (Li) evaporation after the plasma breakdown and the real-time injection of fine Li powder into the plasma edge.

Fig. 2 shows time evolutions of plasma parameters for a typical EAST discharge 38 213 which is operated in the DN configuration since the dR_{sep} is close to 0 (Fig. 2(e)). Here, the dR_{sep} is the radial separation between upper and lower X-points, mapped to the outer midplane with a standard EFIT equilibrium. Therefore, $dR_{sep} > 0$ (< 0) indicates that the upper (lower) X-point is closer to the plasma and hence dominant. A value of $dR_{sep} = 0$ signifies a perfectly balanced DN configuration while a $|dR_{sep}|$ value less than a poloidal ion gyroradius ($\rho_{pi} = \frac{\sqrt{T_i/m_i}}{eB_p/m_i}$) indicates a near-DN configuration. The ρ_{pi} is estimated to be 0.8–1.2 cm in present experiments on EAST and hence a configuration with $dR_{sep} \sim 0$ is considered to be DN and that with $dR_{sep} > 1$ cm is USN while one with $dR_{sep} < -1$ cm indicates a LSN configuration. The auxilliary heating in shot 38 213 is LHW with a power of ∼1 MW. The plasma enters into H-mode at about 2.28 s. The D_α signal is initially at a reduced level compared with L-mode before 2.14 s and then gradually increases. The diamagnetic energy (W_{dia}) and core line averaged density ($\langle n_e \rangle$) show gradually increase after 2.28 s. An intermediate phase (labeled as I phase) with D_α showing dithering cycles or oscillation is observed between 2.14 s and 2.28 s in Fig. 2(d). During this I phase, both W_{dia} and $\langle n_e \rangle$ show

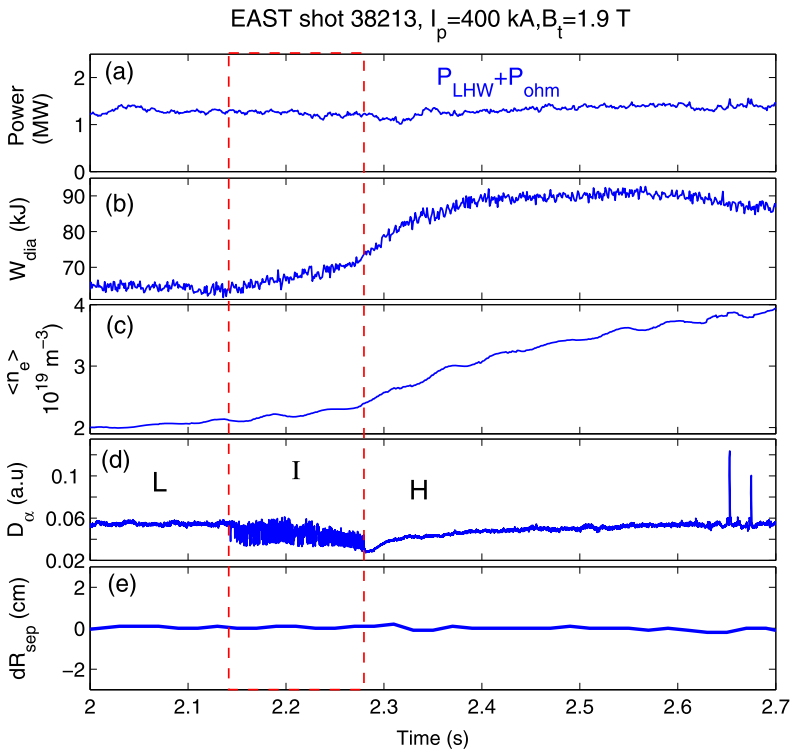

Fig. 2. A typical plasma with L–I–H transition displaying characteristics of dithering during I phase on EAST tokamak (a) the total power from LHW and ohmic heating, (b) diamagnetic energy (W_{dia}), (c) core line averaged density ($\langle n_e \rangle$), (d) Divertor D_α line and (e) dR_{sep}. The dashed rectangular indicates the I phase.

moderate increase, indicating confinement improvement. Following the I phase, the plasma stays in ELM free H-mode up to the appearance of the type-III ELM at about 2.65 s. Fig. 3 shows the magnetic equilibrium reconstructed from EFIT and the toroidal view of a CCD camera measuring the visible light plasma radiation for three different time which corresponding to the L, I and H phase. The DN configuration can be clearly seen in these equilibriums. It can be judged from the EFIT equilibriums and the CCD measurement that the plasma real equilibrium shows no clear change during the L–I–H transition process. In present EAST experiments, several L–H and H-L back transitions in one single shot are usually observed even at the flattop phase of heating power. In this Letter, we only concentrate on the first L–H transition.

The dithering event in I phase is also observed in other diagnostics, as shown in Fig. 4 for shot 40 846 with $\langle n_e \rangle \sim 2.7 \times 10^{19}$ m^{-3}. Poloidal magnetic fluctuation (δb_θ) measured by edge magnetic probe clearly sees the oscillation. The extreme ultraviolet radiation (XUV) close to the edge can also see this oscillation while it cannot be observed in more inside channels of XUV (Fig. 4(c)). This result indicates that the dithering is an edge event. The setups of XUV and other diagnostics on EAST are shown in Fig. 5. Fig. 4(d) shows that the LiII line radiation can see the dithering while the LiI line radiation cannot. This is consistent with the XUV measurement, i.e. the dithering occurring at the edge, since LiII is more close to the edge due to the lower temperature and density. In addition, the density fluctuation measured by a 60 GHz reflectometry at normalized radius ($\rho = r/a$) of ~0.94 shows modulation during the I phase (Fig. 4(e) and (f)). The reflectometry with X-mode polarization is installed in the midplane at low field side on EAST tokamak. The system can be used for the density profile or density fluctuation measurement but cannot measure the two quantities at the same time presently [27]. The operating frequency band of this system for fluctuation measurement is from 50 GHz to 75 GHz and the frequency of the probing wave can be fixed or changed step by step. The wave-number of the turbulence measured by the reflectometry is $k_\perp \sim 0$–3 cm^{-1}, corresponding to $k_\perp \rho_s \sim 0$–0.4. It can be seen in Fig. 4(e) and (f), the fluctuation spectrum is broad and the density fluctuation level ($\delta n/n$) is high at the L phase. When D_α decreases during the I phase, the high frequency fluctuation component is suppressed and the energy converges to zero frequency indicating a lower density fluctuation level [28] while the fluctuation recovers to the L phase level with the increasing of D_α. When plasma enters into the H phase at ~2.728 s, the density fluctuation amplitude keeps at a low level. It is also observed that the oscillation in D_α lags about 100–140 μs behind those seen in above mentioned diagnostic signals. This time lag is consistent with an estimated plasma loss time due to parallel scape-off layer flow $0.5q_{95}R/0.3c_s \approx 120$ μs.

The observations from XUV and LiII radiation measurement have shown that the dithering mainly occurs at the plasma edge. The localization of the dithering has been further studied using the fluctuation reflectometry. An experiment has been done by changing the reflectometry frequency shot by shot in a series of discharges with similar plasma parameters. The plasma density before L–H transition in these shots is $\langle n_e \rangle = 2 \times 10^{19}$ m^{-3}. Six probing frequencies, i.e. 52 GHz, 56 GHz, 60 GHz, 64 GHz, 68 GHz and 72 GHz, are selected for the density fluctuation measurement. Fig. 6 shows the divertor D_α as references and the $\delta n/n$ measured by reflectometry with the six frequencies. All these shots show the I phase with dithering which can be clearly observed in the D_α signals. However, the detailed behavior of these ditherings, e.g. the length, are different. This difference is a usual observation even for the plasmas with the same conditions. Nevertheless, the density fluctuation measured by the 52 GHz, 56 GHz and 60 GHz reflectometry can see the dithering while this oscillation is not observed in the density fluctuation measured by reflectometry with higher frequencies. It is further observed from Fig. 6(c) that the 60 GHz reflectometry in shot 41 707 can see the oscillation only in the later dithering phase while the first three cycles is not clearly observable in the $\delta n/n$ signal. Fig. 7

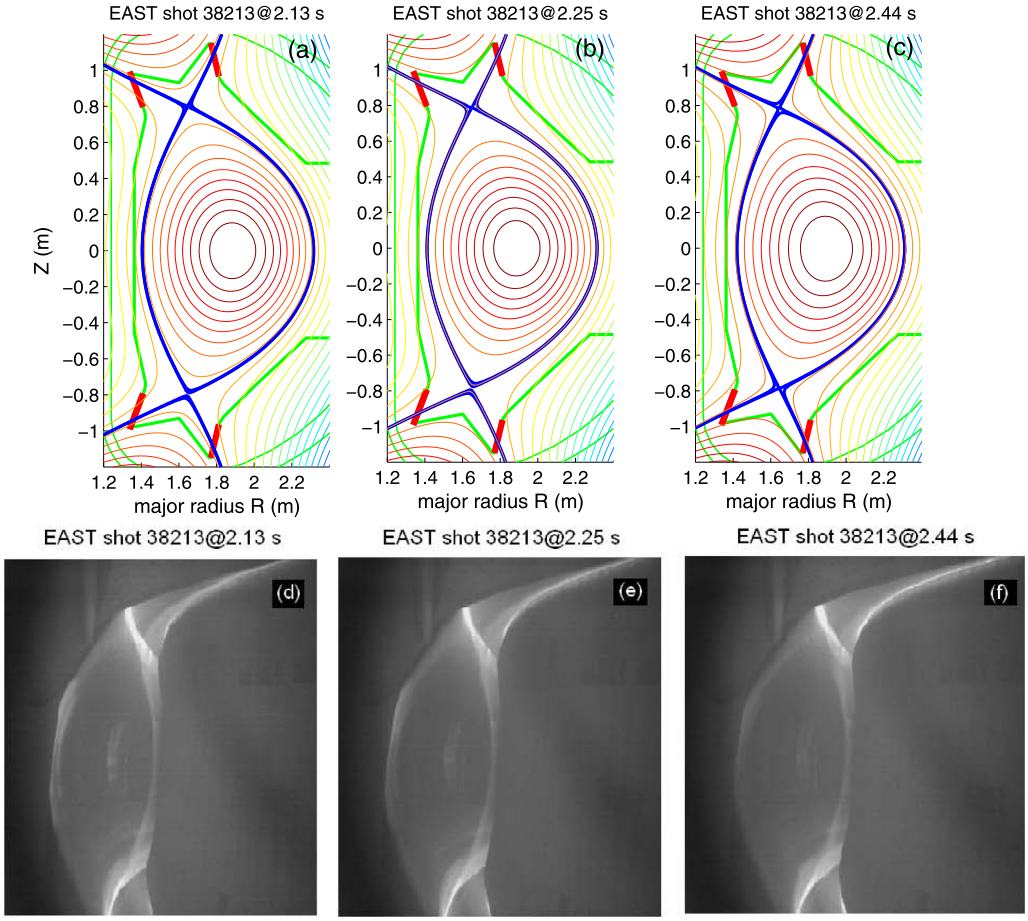

Fig. 3. (a)–(c) EFIT equilibrium reconstruction and (d)–(f) the toroidal view of a CCD camera measuring the visible light plasma radiation for shot 38213 at 2.13 s (L phase), 2.25 s (I phase) and 2.44 s (H phase) respectively.

shows that the outside XUV channels cxuv11d–cxuv16d can see the dithering while more inside channels cannot observe this oscillation. It is also noted that the channel of cxuv11d can see the oscillation only in the later dithering phase which is similar to the observation of the 60 GHz reflectometry. This may be due to that the oscillation affects more inside plasma in the later phase and this effect has been observed in experiment [21] and modeling [29]. But we cannot exclude the explanation that the observation in cxuv11d and 60 GHz reflectometry is due to the density increase during the dithering (Fig. 8) based on present data. Due to the fact mentioned above that the reflectometry cannot measure the density profile and fluctuation at the same time, a similar discharge, 41 554, with the same density is selected to study the localization of the dithering. Fig. 8 shows the density profiles measured by reflectometry at four different time corresponding to the L, early I, later I and H phases respectively and the cutoffs of the reflectometry with the six probing frequencies are also indicated in each profile. It is clearly seen that both edge and core density gradually increase during the I phase which is consistent with the evolution of $\langle n_e \rangle$. In the early I phase, the dithering is observed on 52 GHz and 56 GHz reflectometry which cover 2.285 m $< R <$ 2.3 m and cannot be seen by the reflectometry with frequency larger than 60 GHz which cover $R >$ 2.25 m. In the later I phase, the dithering is observed on 52, 56 and 60 GHz reflectometry which cover 2.29 m $< R <$ 2.3 m and cannot be seen by the reflectometry with frequency larger than 64 GHz which cover $R >$ 2.25 m. Since the signal measured by XUV diagnostics is an integral along the view line (Fig. 5), we have calculated the covered regions for two channels, cxuv11d and cxuv16d, by mapping the view lines of them to the midplane using the EFIT equilibrium. The result shows that the cxuv11d covers the region with $R >$ 2.21 m while cxuv16d covers a region with $R >$ 2.31 m just outside the separatrix ($R =$ 2.308 m). By combining the measurement from reflectometry and XUV, we conclude that the dithering occurs at least 2 cm inside separatrix and extends into SOL region as the shaded rectangular indicated in Fig. 8(c) while the upper limit of the radial extension that this dithering occurs is about 6 cm at the edge. The 'dithering' cycles observed in AUG was also about 2 cm inside the separatrix [17] and the 'IM mode' oscillation observed on DIII-D was principally near separatrix from $\rho = 0.98$–1.0 and extended into the SOL [18, 19].

3. Occurrence of dithering on EAST

Fig. 9(a) summarizes the occurring condition in the parameter space of P_{loss} and dR_{sep} for about 800 discharges in present EAST experiment. Here, $P_{loss} = P_{LHW} + P_{ICRH} + P_{ohm} - dW_{dia}/dt$ is defined as the power loss passing through the separatrix. The density of these discharges is from 2×10^{19} m^{-3} to 4×10^{19} m^{-3}. It can be seen that the discharges with and without dithering are well separated by dR_{sep}. The dithering occurs at DN or USN configurations and no observation of dithering is found in LSN configuration. In the transition configuration between LSN and DN, both kinds of discharge can exists. It is noted there are still several discharges without dithering in the DN configuration. Replacing the P_{loss} with the normalized power in excess of the threshold power P_{scal}, i.e. $(P_{loss} - P_{scal})/P_{scal}$, cannot improve the distribution

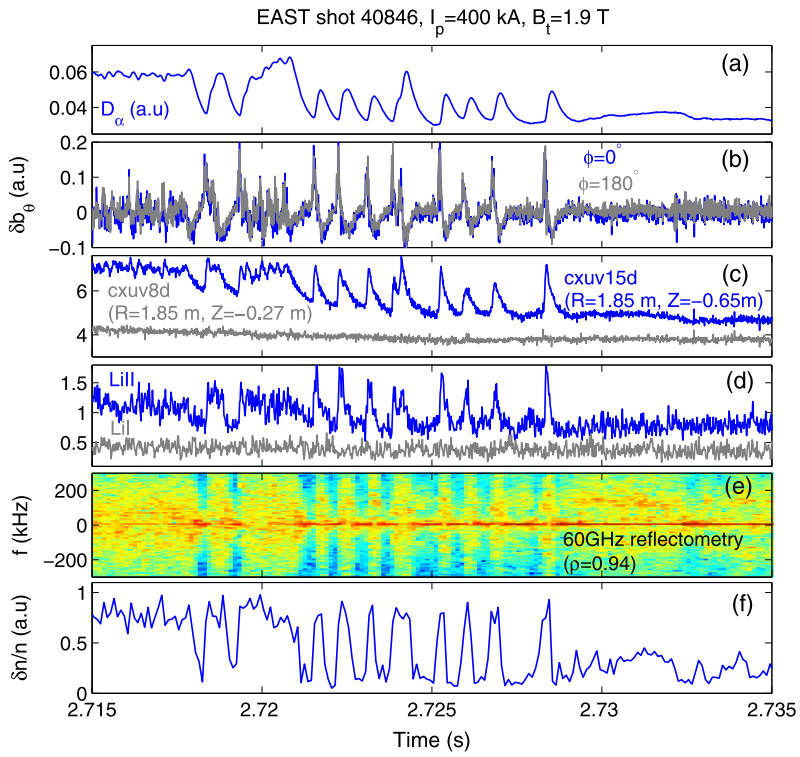

Fig. 4. Observation of dithering from different diagnostics in EAST shot 40 846. (a) divertor D_α as a reference, (b) poloidal magnetic fluctuation δb_θ measured by two magnetic probes at high field side ($R = 1.29$ m, $Z = 0.635$ m) but with a 180° toroidal separation, (c) extreme ultraviolet radiation (XUV) measurement in edge (cxuv15d with $R = 1.85$ m and $Z = -0.65$ m) and core (cxuv8d with $R = 1.85$ m and $Z = -0.27$ m), (d) LiI and LiII line radiation, (e) spectrogram of density fluctuation measured by 60 GHz reflectometry at $\rho \sim 0.94$ and (f) the density fluctuation level measured by this reflectometry.

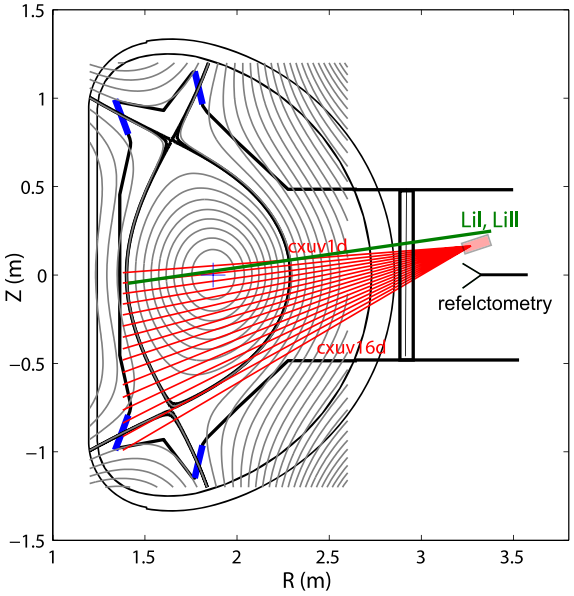

Fig. 5. A schematic of the diagnostics on EAST. cxuv1d–cxuv16d are the 16 channels XUV radiation measurement from core to edge. LiI and LiII are the line radiation from Li^+ and Li^{2+}. Reflectometry is in the midplane at low field side and used to measure the density profile and density fluctuation. The marker of '+' indicates the magnetic axis.

of dithering in the parameter space as shown in Fig. 9(b). Here, $P_{scal} = 0.8 \times P_{08,scal}$ with $P_{08,scal} = 0.049\langle n_{e20}\rangle^{0.72} B_t^{0.8} S^{0.94}$ being the L–H transition power threshold based on the ITPA multi-machine database [30]. The factor 0.8 is taken by considering the fact that the L–H transition power threshold with molybdenum wall on EAST is smaller than the scaling $P_{08,scal}$ by a factor of about 20% [31]. It is noted that the threshold power is also reduced by about 25% to 30% on JET when the first walls are changed from carbon walls to metal walls [32]. As mentioned in Section 2, the $B \times \nabla B$ direction in USN is 'favorable' while it is 'unfavorable' in LSN configuration for the data presented in Fig. 9. The study has shown that the threshold power in DN is smaller than that in LSN by a factor about 30% to 40% on EAST [31]. Some evidences also show that the threshold power in USN is smaller than that LSN and larger than that in DN, but this point needs further confirmation in future. Fig. 10 shows that the dithering is clearly observed in D_α preceding the L–H transition in the plasma with DN configuration. For the plasma in LSN configuration, there exists irregular fluctuation with much smaller amplitude preceding the L-H transition. This fluctuation is similar to that observed in previous EAST experiment [24] and also resembles the so-called 'L-mode fluctuation' observed in AUG [17]. It has shown in AUG that the 'dithering' cycles can be observed only in the plasma with 'favorable' direction while the 'L-mode fluctuation' was usually observed in the D_α signal when plasma is in 'unfavorable' direction [17].

Fig. 11(a) and (b) show the dependence of the dithering length (Δt_{dither}) on the normalized power in excess of the threshold power for two different density ranges. The data is scattering and no clear dependence is observed. Nevertheless, the distribution of Δt_{dither} is broader in the plasma with heating power closer to the threshold power, e.g. that the Δt_{dither} can be from several *ms* up to 200 ms when $(P_{loss} - P_{scal})/P_{scal} < 0.5$ while the Δt_{dither} is less than 50 ms for most discharges when $(P_{loss} - P_{scal})/P_{scal} > 0.5$. It was shown that the length of the 'dithering' cycles in AUG decreased with the ramp rate γ_P of the power in excess of the L–H transition threshold power [16]. On EAST, the L–H transition usually occurs at the flattop phase of the heating power (e.g. Fig. 2). It is difficult to define the ramp rate of the heating power. Here, we use the energy confinement time τ_E as an

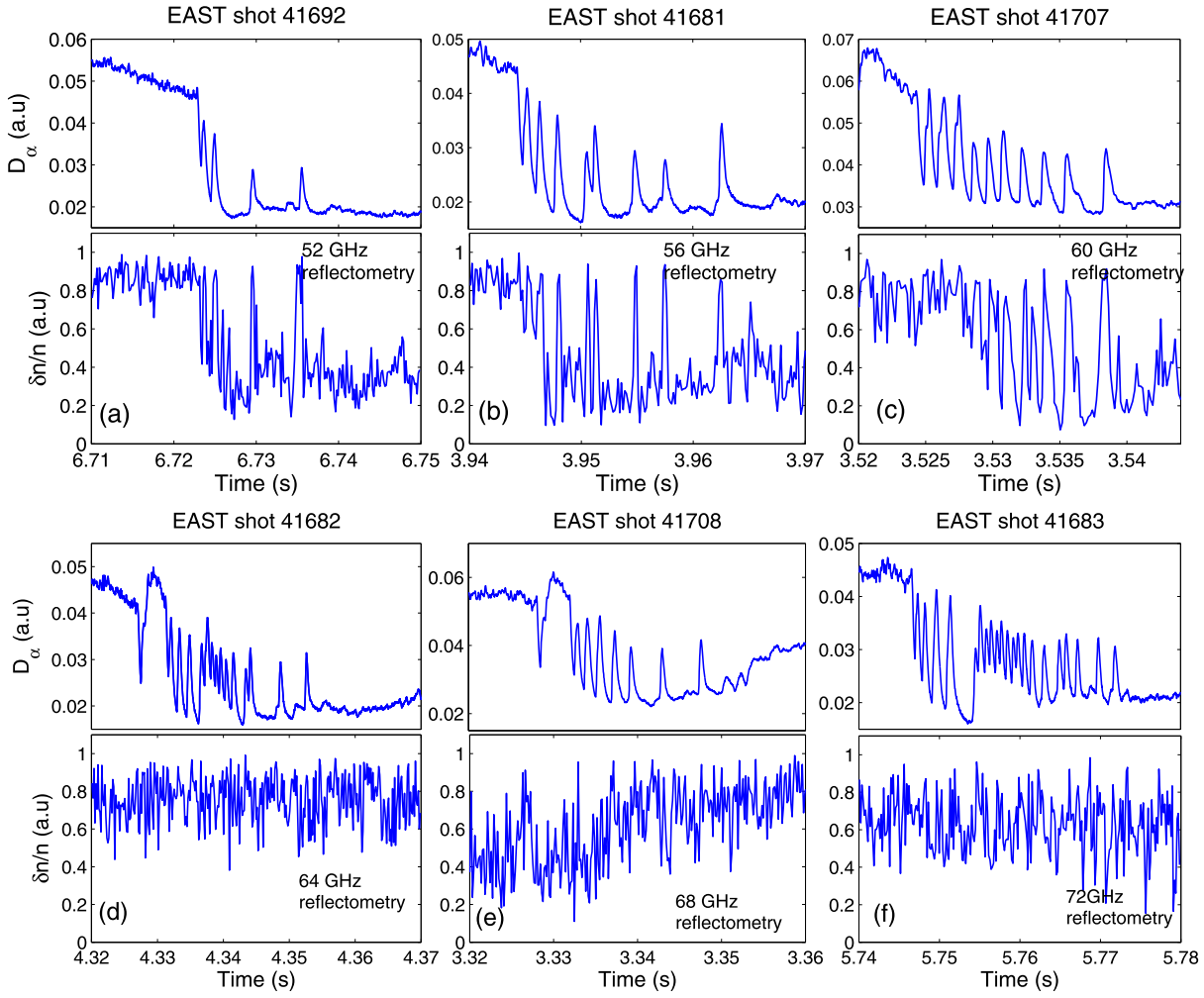

Fig. 6. Density fluctuation measurement by reflectometry with 6 different probing frequencies. The upper plots in (a)–(f) show the divertor D_α signals as references and the lower plots show the $\delta n/n$.

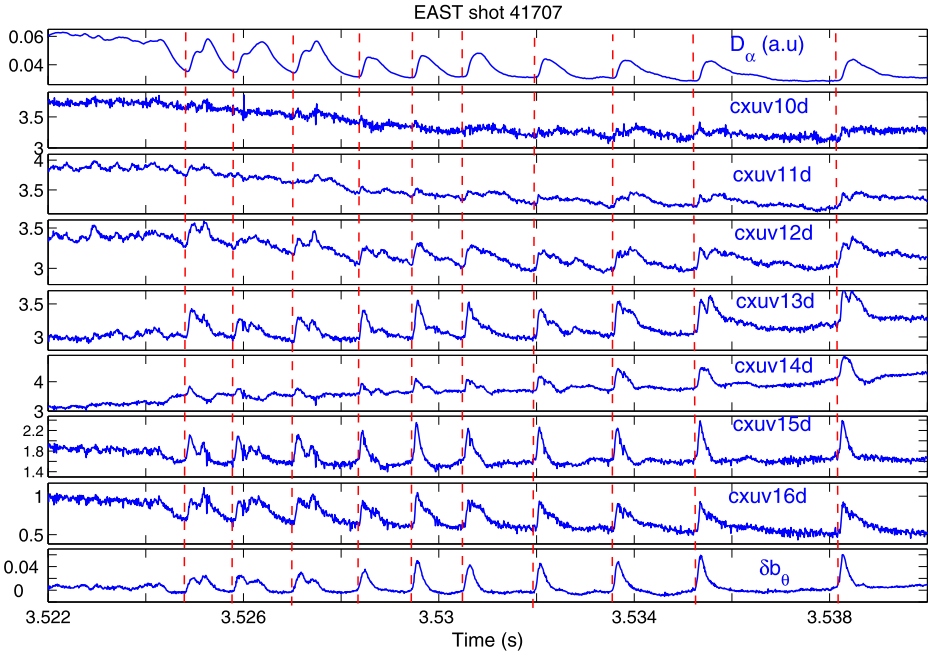

Fig. 7. From top to bottom are divertor D_α signal, XUV channels from inner to outer region cxuv10d–cxuv16d and δb_θ measured by edge magnetic probe for EAST shot 41 707.

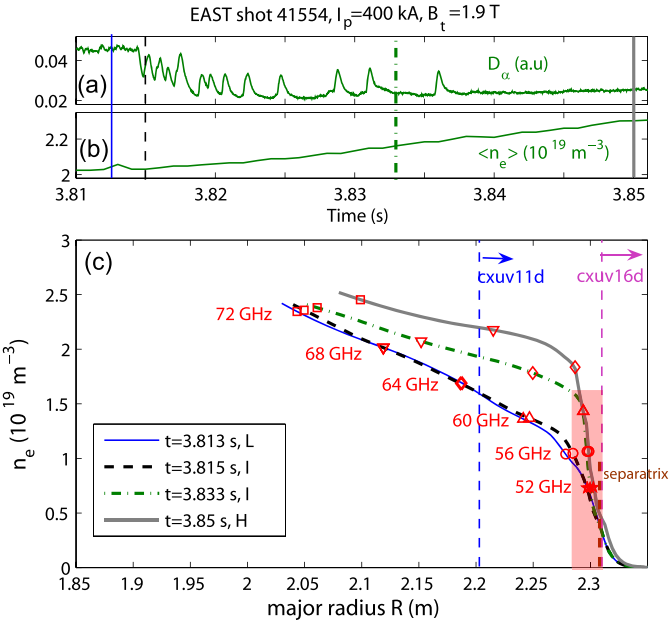

Fig. 8. EAST shot 41 554: (a) D_α signal, (b) $\langle n_e\rangle$ and (c) density profiles at four different time (indicated by vertical lines in (a) and (b)) corresponding to L phase, early I phase, later I phase and H phase respectively. The markers indicate the cut-offs of the reflectometry. The covered regions for two XUV channels, cxuv11d and cxuv16d, are from edge to the radial positions indicated by the two long vertical dash lines respectively. The short and bold dash line indicates the position of separatrix. The shaded rectangular indicates the occurring region of dithering deduced from reflectometry and XUV measurement.

indication of the time scale. Fig. 11(c) and (d) show the dependence of Δt_{dither} on $\gamma_P = (P_{loss} - P_{scal})/(P_{scal}\tau_E)$. Compared to Fig. 11(a) and (b), no further improvement on the dependence can be achieved by doing so. Fig. 12 shows that three neighboring shots have similar parameters but the dithering lengths are different. It is still unclear what parameter controls the dithering length on EAST.

4. Plasma evolution during dithering

It can be seen in Fig. 12 that the increasing rate of W_{dia} and $\langle n_e\rangle$ during the I phase is smaller in the plasma with longer dithering length. Fig. 13 shows the dependence of dW_{dia}/dt and $d\langle n_e\rangle/dt$ on the Δt_{dither} for all the discharges in database. Here, the dW_{dia}/dt ($d\langle n_e\rangle/dt$) is the increasing rate of W_{dia} ($\langle n_e\rangle$) and calculated by the increment of W_{dia} ($\langle n_e\rangle$) during the I phase divided by Δt_{dither}. It can be seen from the Figure that both increasing rates of energy and density during the I phase decrease with the increasing of the dithering length. It is further observed in Fig. 12(b) that the plasma enters in the H-mode once the W_{dia} arrive at the value of about 74 kJ for all the three shots while the Δt_{dither} are different. Since diamagnetic energy is directed linked to the plasma pressure, this result may imply that a critical pressure or pressure gradient are needed to finally lock the specific plasma in H-mode. This will be investigated in future after the upgrade of the plasma edge diagnostics on EAST.

The evolution of density profiles during the I phase has been studied using the reflectometry system (Fig. 5). In fact, there are two types of dithering observed on EAST. Fig. 14(a)–(e) show the first type dithering where the W_{dia}, $\langle n_e\rangle$, n_e^{ped} and maximum ∇n_e ($\max(\nabla n_e)$) don't change in the early dithering phase and begin to increase in the later dithering phase. Here, the n_e^{ped} and $\max(\nabla n_e)$ are calculated as follows: the density profiles (e.g. Fig. 14(f)) measured by the reflectometry is fitted by the modified hyperbolic tangent (MTANH) function [33]. The density pedestal height n_e^{ped}

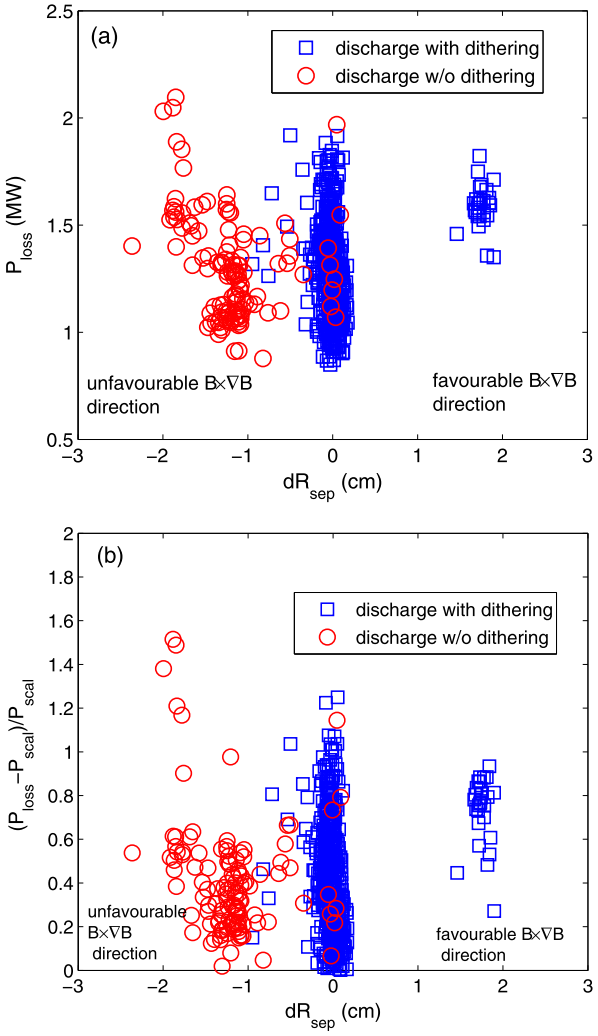

Fig. 9. The occurring condition of dithering on EAST parameter space of (a) P_{loss} and dR_{sep} and (b) $(P_{loss}-P_{scal})/P_{scal}$ and dR_{sep}.

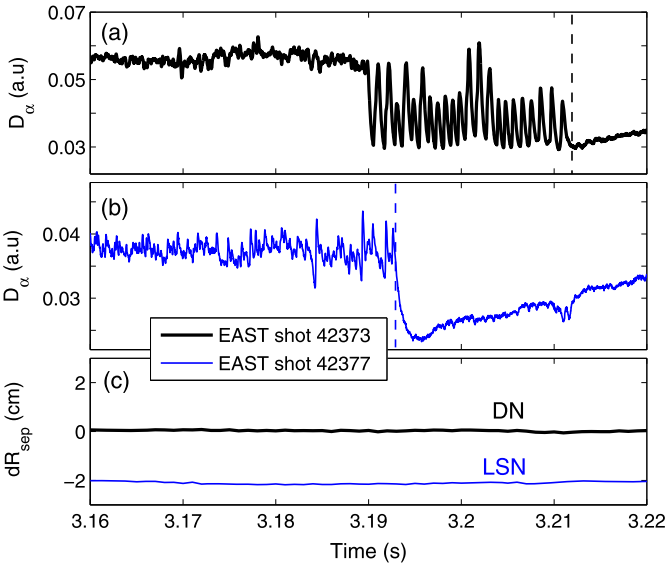

Fig. 10. An example to show the difference of D_α signal during L–H transition between the DN and LSN configurations. (a) D_α in shot 42 373 with DN, (b) D_α in shot 42 377 with LSN and (c) dR_{sep} in the two shots. The dashed vertical lines in (a) and (b) indicate the time of L–H transition for each shot.

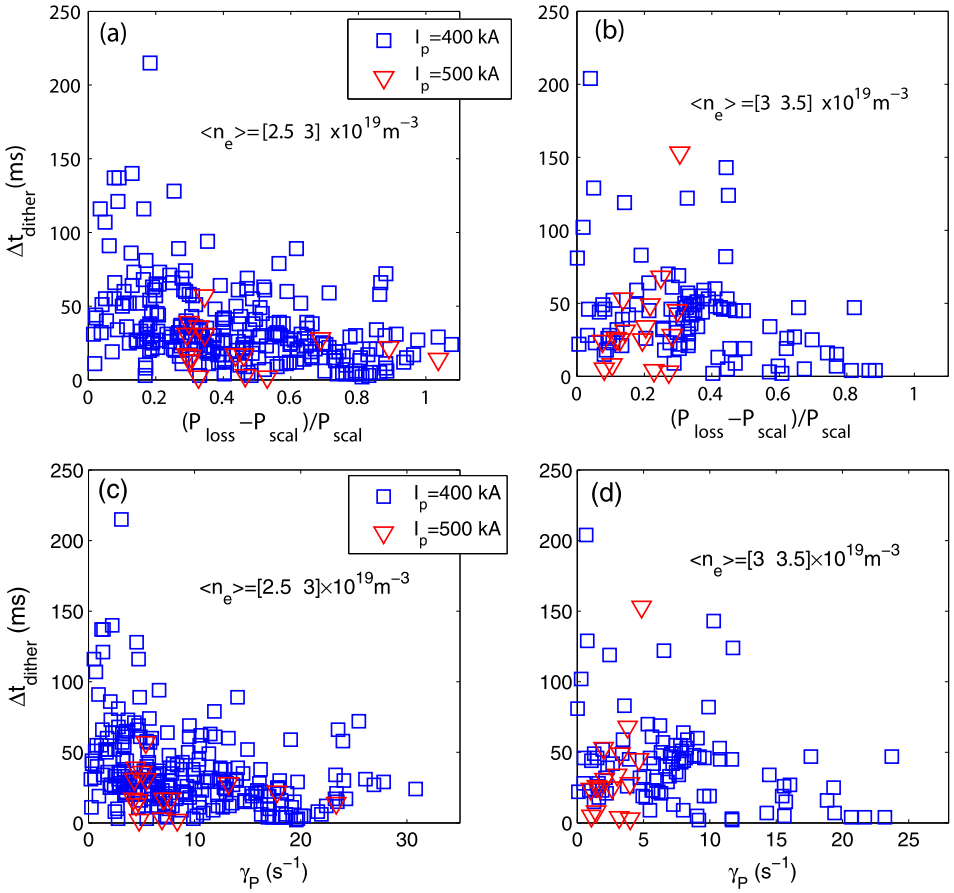

Fig. 11. The dependence of dithering length (Δt_{dither}) on $(P_{loss} - P_{scal})/P_{scal}$ in (a) and (b) and on $\gamma_P = (P_{loss} - P_{scal})/(P_{scal}\tau_E)$ in (c) and (d).

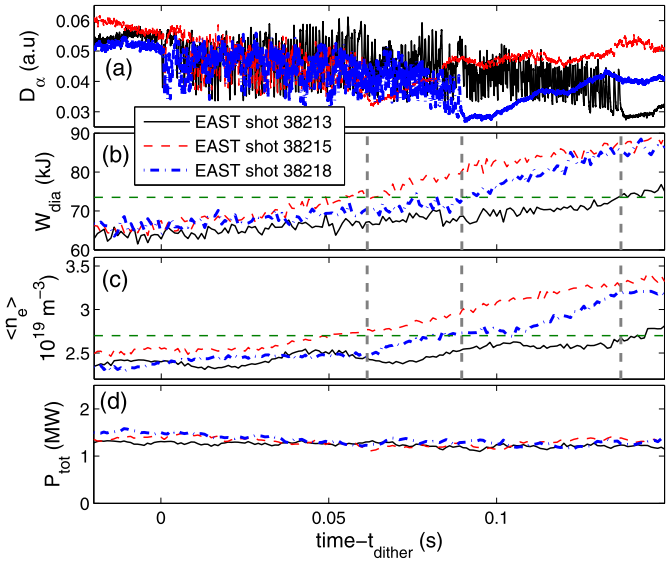

Fig. 12. Three shots with similar parameters have different dithering length. (a) D_α, (b) W_{dia}, (c) $\langle n_e \rangle$ and (d) total heating power P_{tot}.

can be directly calculated using the fitting parameters and the $\max(\nabla n_e)$ is the maximum density gradient of the fitting profile. The quantity of n_e^{ped} is used to indicate how the edge density evolves during the I phase. The boundary of the early and later dithering phase for this shot 41 386 is at about 4.112 s which has been indicated by a vertical dash line in these figures. Fig. 14(f) shows that the density profiles in early dithering phases are similar to that in L phase while the density and density gradient in later dithering phase gradually increase. As discussed in Section 2, the decreasing phase of D_α nearly corresponds the density fluctuation suppression phase except that there is short time delay of about 100–140 μs. Taking the D_α signal as reference, it can be seen in Fig. 14(a) that the time D_α stays in the L phase value is larger than that of D_α decreasing, i.e. the time that edge plasma with L mode turbulence level larger than that plasma with turbulence suppression, in the early dithering phase. On the other hand, the time edge plasma stays in the turbulence suppression phase is larger than that plasma with L mode turbulence level in the later dithering phase. This may explain why the plasma energy and density show increase in the later dithering phase and no changes of the two quantities in the early dithering phase. The density profile when plasma evolves into type-III ELMy H mode is also shown in Fig. 14(f) for comparison. The pedestal top cannot be seen by the present reflectometry system due to the limitation of the probing frequency [27]. The pedestal height should be at least 2.7×10^{19} m^{-3}, much larger than that during the I phase which is less than 2×10^{19} m^{-3}. This is the first difference between the dithering and the type-III ELM, both of which show bursts in D_α signal. A high frequency coherent mode is usually observed before type-III ELM. The mode frequency was born about 150 kHz and gradually decreases up to the ELM. For dithering, the high frequency turbulence is usually suppressed and no coherent mode is observed before the oscillating burst as shown in Fig. 4(e). This is second difference between dithering and type-III ELM on EAST.

Fig. 15(a)–(e) show the second type dithering in shot 41 385. The W_{dia}, $\langle n_e \rangle$, n_e^{ped} and $\max(\nabla n_e)$ begin to increase when plasma evolve into the I phase with dithering at about 3.398 s as indicated

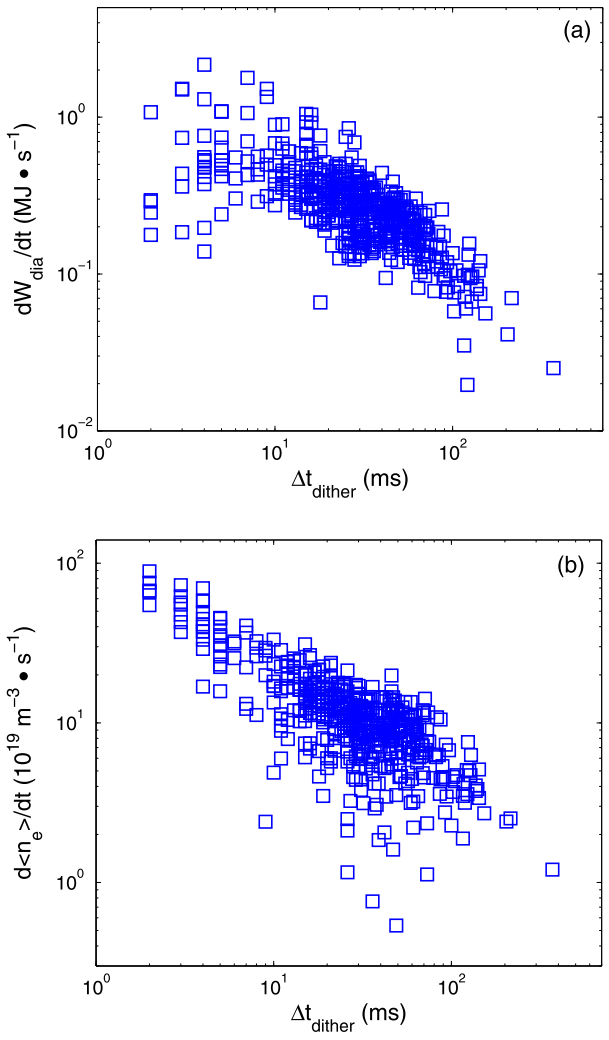

Fig. 13. The dependence of (a) the increasing rate of W_{dia}, dW_{dia}/dt and (b) the increasing rate of $\langle n_e \rangle$, $d\langle n_e \rangle/dt$ on the dithering length during the I phase.

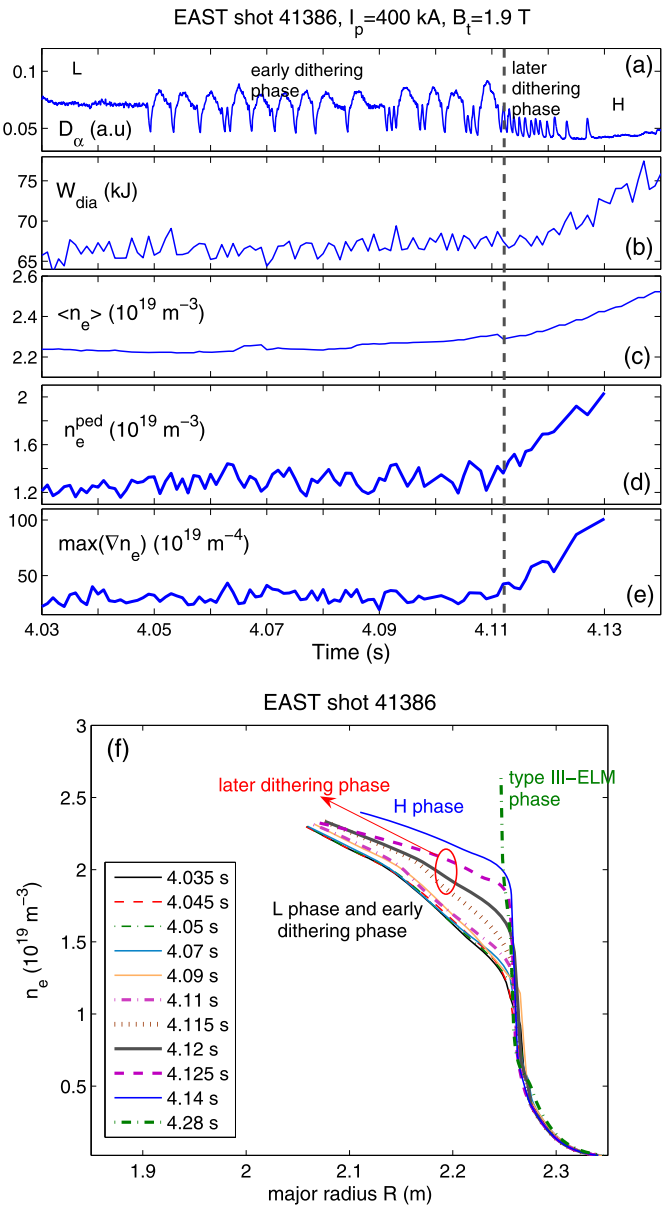

Fig. 14. Evolution of (a) D_α signal, (b) W_{dia}, (c) $\langle n_e \rangle$, (d) n_e^{ped} and (e) maximum n_e gradient, max(∇n_e) for EAST shot 41 386. The vertical dashed line separates the early dithering and later dithering phase. (f) shows the density profiles measured by reflectometry during the L–I–H transition. The profile in type-III ELMy H-mode phase is also shown for comparison.

by a vertical dash line in these figures. Fig. 15(f) shows that the edge density and density gradient continuously increase during the dithering phase. This is due to that the plasma stays in the turbulence suppression phase longer than in the L-mode turbulence level especially for the later several cycles shown in Fig. 15(a).

5. Discussion and summary

A comparison between the characteristics of dithering observed on EAST and similar oscillations preceding the L–H transition in other devices is performed. Firstly, the dithering on EAST mainly occurs at least about 2 cm just inside the separatrix and extends into SOL. This is similar to the 'dithering' cycles in AUG [17] and the 'IM mode' in DIII-D [19] but different from the so-called 'L–H cycles' observed on H-1 Heliac [22] where the perturbation can affect the whole plasma. This has been attributed to the global nature of the fluctuations in H-1 [22]. Actually, the edge density fluctuation is periodically suppressed during the dithering phase on EAST while no suppression of turbulence is observed more inside the plasma as shown in Fig. 6. This periodical suppression of the edge fluctuation level in the I phase is also observed in the simulation [29]. Secondly, the dithering cannot be observed in plasma with LSN configuration, i.e. 'unfavorable' $B \times \nabla B$ direction, on EAST. The 'dithering' cycles on AUG also cannot be seen in the plasma with 'unfavorable' direction [17]. In addition, the small irregular fluctuation preceding the L–H transition observed in the LSN configuration on EAST (Fig. 10(b)) resembles the 'L-mode fluctuation' seen on AUG when the B_t was reversed and the $B \times \nabla B$ drift was in the 'unfavorable' direction. Lastly, the density profiles gradually evolves during the whole dithering phase or later dithering phase depending on the type of dithering one EAST. This is different from the 'IM mode' on DIII-D where the density profiles nearly show no change during the 'IM mode' phase while the temperature profiles slowly evolve due to the gradual increase of heating power [19]. The first type of dithering on EAST where the energy and density show no change in the early dithering phase and gradually increase in the later dithering phase (Fig. 14) is similar to the 'dithering' cycles on AUG [17]. We conclude from the comparison that the characteristics of dithering on EAST is most similar to the 'dithering' cycles observed on AUG. However, the differences between them are evident. Firstly, the length of the 'dithering' cycles increases with the decreasing of the power ramp

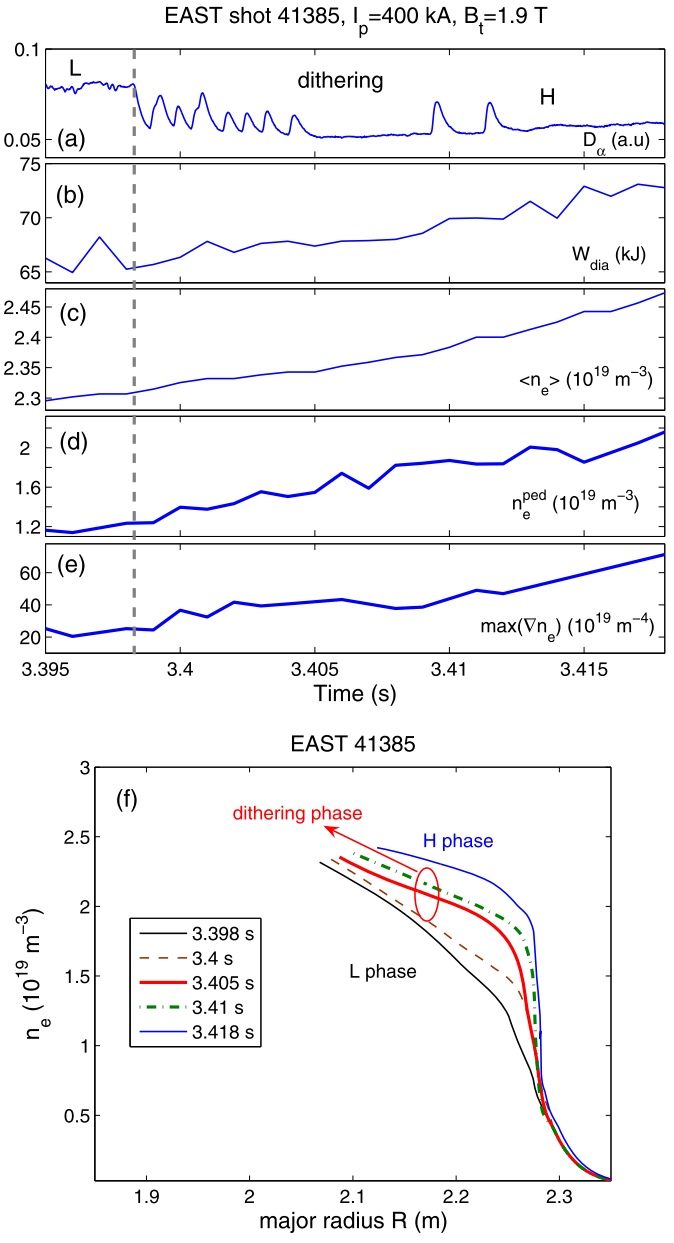

Fig. 15. Evolution of (a) D_α signal, (b) W_{dia}, (c) $\langle n_e \rangle$, (d) n_e^{ped} and (e) maximum n_e gradient, max(∇n_e) for EAST shot 41 385. The vertical dashed line indicates the time at which the plasma enters into the I phase and both energy and density begin to increase. (f) shows the density profiles measured by reflectometry during the L–I–H transition.

rate on AUG while the length of dithering has no clear dependence on the heating power on EAST. Secondly, the 'dithering' cycles on AUG was usually observed in plasma with marginal input power and the 'L-mode fluctuation' appeared in the plasma with high heating power. On EAST, the dithering can be still observed even the factor of the heating power in excess of the threshold power is larger than 100% as shown in Fig. 9(b). The origin of the difference may come from the different heating methods. Presently, the H-mode is achieved mainly using LHW or LHW + ICRH while it is difficult to trigger L–H transition using ICRH solely on EAST. The ICRH heating system will be upgraded and a new neutral beam injection system will be installed in next EAST campaign. It is deserved to study the effects of different heating methods on the dithering characteristics in the future.

In summary, dithering cycles preceding the L–H transition has been observed and experimentally characterized on EAST tokamak. The dithering occurs in plasma with DN and USN configuration and cannot be observed in LSN configuration where the ion $B \times \nabla B$ drift directions is away from the X-point, i.e. 'unfavorable' direction. The dithering affects the plasma at least 2 cm inside the separatrix and extends into the SOL. The dithering length (Δt_{dither}) has no clear dependence on the heating power. Generally, the plasma stored energy and density gradually increase during the dithering phase and the increasing rates of them decreases with the increasing of Δt_{dither}. There are two types of dithering. In the first type, the energy, density and density gradient shows no change in the early dithering phase but slowly increase in the later dithering phase. In the second type, these quantities begin to increase once the plasma evolves into the I phase with dithering. The confinement improvement in the later dithering phase of first type dithering or in the second type dithering has been attributed to that the edge plasma stays in turbulence suppression phase longer than in L-mode turbulence level phase.

Acknowledgements

This work was supported by National Magnetic Confinement Fusion Program of China (Nos. 2010GB106000 and 2010GB106001) and the National Natural Science Foundation of China (Nos. 11021565 and 11275234).

References

[1] F. Wagner, G. Becker, K. Behringer, D. Campbell, A. Eberhagen, W. Engelhardt, G. Fussmann, O. Gehre, J. Gernhardt, G.v. Gierke, G. Haas, M. Huang, F. Karger, M. Keilhacker, O. Klüber, M. Kornherr, K. Lackner, G. Lisitano, G.G. Lister, H.M. Mayer, D. Meisel, E.R. Müller, H. Murmann, H. Niedermeyer, W. Poschenrieder, H. Rapp, H. Röhr, F. Schneider, G. Siller, E. Speth, A. Stäbler, K.H. Steuer, G. Venus, O. Vollmer, Z. Yü, Phys. Rev. Lett. 49 (1982) 1408.
[2] F. Wagner, Plasma Phys. Control. Fusion 49 (2007) B1.
[3] J.W. Connor, H.R. Wilson, Plasma Phys. Control. Fusion 42 (2000) R1.
[4] K.H. Burrell, T.N. Carlstrom, E.J. Doyle, P. Gohil, R.J. Groebner, T. Lehecka, N.C. Luhmann, H. Matsumoto, T.H. Osborne, W.A. Peebles, R. Philipona, Phys. Fluids B 2 (1990) 1405.
[5] E.J. Doyle, R.J. Groebner, K.H. Burrell, P. Gohil, T. Lehecka, N.C. Luhmann, H. Matsumoto, T.H. Osborne, W.A. Peebles, R. Philipona, Phys. Fluids B 3 (1991) 2300.
[6] C.L. Rettig, W.A. Peebles, K.H. Burrell, E.J. Doyle, R.J. Groebner, N.C. Luhmann Jr., R. Philipona, Nucl. Fusion 33 (1993) 643.
[7] G.R. Tynan, L. Schmitz, L. Blush, J.A. Boedo, R.W. Conn, R. Doerner, R. Lehmer, R. Moyer, H. Kugel, R. Bell, S. Kaye, M. Okabayashi, S. Sesnic, Y. Sun, Phys. Plasmas 1 (1994) 3301.
[8] R.A. Moyer, K.H. Burrell, T.N. Carlstrom, S. Coda, R.W. Conn, E.J. Doyle, P. Gohil, R.J. Groebner, J. Kim, R. Lehmer, W.A. Peebles, M. Porkolab, C.L. Rettig, T.L. Rhodes, R.P. Seraydarian, R. Stockdale, D.M. Thomas, G.R. Tynan, J.G. Watkins, Phys. Plasmas 2 (1995) 2397.
[9] S.I. Itoh, K. Itoh, Phys. Rev. Lett. 60 (1988) 2276.
[10] K.C. Shaing Jr., E.C. Crume, Phys. Rev. Lett. 63 (1989) 2369.
[11] A.B. Hassam, T.M. Antonsen Jr., J.F. Drake, C.S. Liu, Phys. Rev. Lett. 66 (1991) 309.
[12] H. Biglari, P.H. Diamond, P.W. Terry, Phys. Fluids B 2 (1990) 1.
[13] P.H. Diamond, Y.M. Liang, B.A. Carreras, P.W. Terry, Phys. Rev. Lett. 72 (1994) 2565.
[14] E.J. Kim, P.H. Diamond, Phys. Rev. Lett. 90 (2003) 185006.
[15] E.J. Kim, P.H. Diamond, Phys. Plasmas 10 (2003) 1698.
[16] H. Zohm, Phys. Rev. Lett. 72 (1994) 222.
[17] H. Zohm, W. Suttrop, K. Büchl, H.J. de Blank, O. Gruber, A. Kallenbach, V. Mertens, F. Ryter, M. Schittenhelm, ASDEX Upgrade Team, ICRH Group, NBI Group, Plasma Phys. Control. Fusion 37 (1995) 437.
[18] R.J. Colchin, M.J. Schaffer, B.A. Carreras, G.R. McKee, R. Maingi, T.N. Carlstrom, D.L. Rudakov, C.M. Greenfield, T.L. Rhodes, E.J. Doyle, N.H. Brooks, M.E. Austin, Phys. Rev. Lett. 88 (2002) 255002.
[19] R.J. Colchin, B.A. Carreras, R. Maingi, L.R. Baylor, T.C. Jernigan, M.J. Schaffer, T.N. Carlstrom, N.H. Brooks, C.M. Greenfield, P. Gohil, G.R. McKee, D.L. Rudakov, T.L. Rhodes, E.J. Doyle, M.E. Austin, J.G. Watkins, Nucl. Fusion 42 (2002) 1134.
[20] G.D. Conway, C. Angioni, F. Ryter, P. Sauter, J. Vicente, ASDEX Upgrade Team, Phys. Rev. Lett. 106 (2011) 065001.

[21] L. Schmitz, L. Zeng, T.L. Rhodes, J.C. Hillesheim, E.J. Doyle, R.J. Groebner, W.A. Peebles, K.H. Burrell, G. Wang, Phys. Rev. Lett. 108 (2012) 155002.
[22] D.L. Rudakov, M.G. Shats, J.H. Harris, B.D. Blackwell, Plasma Phys. Control. Fusion 43 (2001) 559.
[23] T. Estrada, C. Hidalgo, T. Happel, P.H. Diamond, Phys. Rev. Lett. 107 (2011) 245004.
[24] G.S. Xu, B.N. Wan, H.Q. Wang, H.Y. Guo, H.L. Zhao, A.D. Liu, V. Naulin, P.H. Diamond, G.R. Tynan, M. Xu, R. Chen, M. Jiang, P. Liu, N. Yan, W. Zhang, L. Wang, S.C. Liu, S.Y. Ding, Phys. Rev. Lett. 107 (2011) 125001.
[25] G.S. Xu, B.N. Wan, J.G. Li, X.Z. Gong, J.S. Hu, J.F. Shan, H. Li, D.K. Mansfield, D.A. Humphreys, V. Naulin, for EAST Team and International Collaborators, Nucl. Fusion 51 (2011) 072001.
[26] Z.X. Liu, X. Gao, W.Y. Zhang, J.G. Li, X.Z. Gong, Y.X. Jie, S.B. Zhang, L. Zeng, N. Shi, EAST Team, Plasma Phys. Control. Fusion 54 (2012) 085005.
[27] S.B. Zhang, X. Gao, B.L. Ling, Y.M. Wang, T. Zhang, X. Han, Z.X. Liu, J.L. Bu, J.G. Li, EAST Team, Plasma Sci. Technol. (2013), in press.
[28] G.J. Kramer, R. Nazikian, E. Valeo, Rev. Sci. Instrum. 74 (2003) 1421.
[29] K. Miki, P.H. Diamond, Ö.D. Gürcan, G.R. Tynan, T. Estrada, L. Schmitz, G.S. Xu, Phys. Plasmas 19 (2012) 092306.
[30] Y.R. Martin, T. Takizuka, ITPA CDBM H-mode Threshold Database Working Group, J. Phys.: Conf. Ser. 123 (2008) 012033.
[31] Z.X. Liu, X. Gao, X.Q. Xu, T.Y. Xia, S.C. Liu, I. Joseph, M. Bill, G.Q. Li, T. Zhang, S.B. Zhang, Y.M. Wang, X. Han, J.G. Li, Nucl. Fusion (2013), submitted for publication.
[32] C.F. Maggi, G. Calabro, E. Delabie, M. Groth, N. Hawkes, E. De la Luna, M. Lehnen, E. Lerche, K. McCormick, F. Militello, C. Reux, F. Rimini, E. Solano, V. Bobkov, M. Brix, A. Czarnecka, J. Flanagan, S. Marsen, I. Nunes, B. Sieglin, D. Van Ester, JET EFDA Contributors, in: 39th EPS Conference on Plasma Physics, 2–6 July 2012, Stockholm, Sweden.
[33] R.J. Groebner, D.R. Baker, K.H. Burrell, T.N. Carlstrom, J.R. Ferron, P. Gohil, L.L. Lao, T.H. Osborne, D.M. Thomas, W.P. West, J.A. Boedo, R.A. Moyer, G.R. McKee, R.D. Deranian, E.J. Doyle, C.L. Rettig, T.L. Rhodes, J.C. Rost, Nucl. Fusion 41 (2001) 1789.